Supporting Information

Thermo-Responsive Hydrophilic Amine Microcapsules for All-in-one Epoxy System: Effective Adhesion, Radiative Cooling, and Toughening via Interpenetrating Networks

Zhaoxin Li [1], Xingrui Liu [1], Zhuang Du [4], Jinglei Yang [1,2,3]

Zhaoxin Li [1], Xingrui Liu [1], Zhuang Du [3], Jinglei Yang [1,2]

[1]Department of Mechanical and Aerospace Engineering, The Hong Kong University of Science and Technology, Clear Water Bay, Kowloon, Hong Kong SAR

[2]HKUST Shenzhen-Hong Kong Collaborative Innovation Research Institute, Futian, Shenzhen, China

[3]Center for Engineering Materials and Reliability, HKUST Fok Ying Tung Research Institute, Guangzhou 511458, China

[4]Guangzhou Lushan New Materials Co., Ltd, Guangzhou 511458, China

Corresponding authors: maeyang@ust.hk

Characterization:

Appearance and release performance evaluation: The pristine microcapsules and FITC-dyed PEW@TEPA microcapsules were observed with an OLYMPUS BX43 optical microscope (OM) with Fluorescence Filter Set for Green Fluorescence Protein (GFP). For the heat trigger release test, the FITC-dyed PEW@TEPA microcapsules were placed on a self-made heating device, including a polyimide (PI) heating film, an AC power supply, a programmable temperature control microcontroller, and a thermocouple for calibrating temperature. After heating at specific temperatures for a certain period, the changes in appearance of the microcapsules were observed and recorded. FITC has excitation and emission spectrum peak wavelengths of approximately 495 nm and 519 nm, giving it a green color. The diameter distributions of the microcapsules were derived from the statistical sizes of at least 200 individual microcapsules using Image J in OM images.

Interfacial tension test: The interfacial tension relationship between each two immiscible liquids in these systems were measured using the pendant drop method with a Biolin THETA T200 machine at room temperature. One liquid was manually dropped into the other immiscible liquid using plastic syringes and needles. Due to the balance of gravity and surface tension, the droplet can stay in a pendant shape. An integrated high-speed camera system was used to analyze the shape of the drop and determine the shape factor based on the Young-Laplace equation.

General characterization of the microcapsules: The surface morphology and shell thickness of the microcapsules, as well as the adhesive failure faces, were characterized using scanning electron microscopy (SEM, JEOL 6700F) with an acceleration voltage of 5.0 kV. Thermogravimetric analysis was performed using a thermogravimetric analyzer (TGA Q5000 Infrared Thermogravimetric Analyzer, USA) in a nitrogen atmosphere. Differential scanning calorimetry (DSC) was conducted using a DSC 2500 (TA Instrument) at a heating rate of 5 °C/min from -20 to 130 °C under a nitrogen atmosphere. XPS analysis (T KRATOS XSAM 800 XPS) was used to reveal the flame retardancy mechanism. The XPS analysis used Al Kα excitation radiation (1,486.6 eV) and set the operating power to 150 W. The X-ray beam spot of the XPS

analysis is 500 μm, and the pass energy is 30 eV.

Mechanical performance test for adhesives: The comprehensive mechanical performance test was conducted by ASTM D1876 (T-Peel test evaluate), ASTM D 1002 (Single lap shear test), and ISO 6922 (Butt joint test), showing the peel, shear and tensile strength of adhesion, respectively. The adhesive strength test was performed in a high-precision tensile machine (UTM-E43), and the test details followed the universal standard. All samples were tested 3 times.

Optical properties for radiative cooling: The spectral reflectance ρ(λ) and transmittance c in the wavelength range of ultraviolet, visible light, and near-infrared (0.3~2.5 μm) were measured using a polytetrafluoroethylene integrating sphere UV-Visible-Near-Infrared spectrophotometer (Hitachi U-4100, Japan). Infrared wavelengths within the range of the integrating sphere, combined with the gold coating in the FTIR spectrometer (Nicolet 6700, Thermo Fisher Scientific, USA), have been characterized. According to Kirchhoff's law, the spectral absorptivity (α(λ)) and emissivity (ε(λ)) of any object in thermal equilibrium must be equal. Therefore, ε(λ)=1-ρ(λ)-τ(λ).

The average solar reflectivity ($\bar{R}_{Solar}$) is defined as:

$$\bar{R}_{Solar} = \frac{\int_{0.3\mu m}^{2.5\mu m} I_{Solar}(\lambda) * R_{Solar}(\lambda,\theta) d\lambda}{\int_{0.3\mu m}^{2.5\mu m} I_{Solar}(\lambda) d\lambda}$$

Where λ is the wavelength of incident light in the range of 0.3-2.5 μm, $I_{Solar}$is the normalized ASTMG173 global solar intensity spectra and $R_{Solar}$is the spectral reflectance of the coating surface.

The average emissivity ($\bar{\varepsilon}_{LWIR}$) in the long-wave infrared atmospheric transmittance window is defined as:

$$\bar{\varepsilon}_{LWIR} = \frac{\int_{8\mu m}^{13\mu m} I_{BB}(\lambda) * \varepsilon_{LWIR}(\lambda,\theta) d\lambda}{\int_{8\mu m}^{13\mu m} I_{BB}(\lambda) d\lambda}$$

Where, I_{BB} is the spectral intensity of blackbody emission, $\varepsilon_{LWIR}$is the angular spectral thermal emissivity of the composite textiles in the range of 8-13μm.

Cooling characterization involved using 16×16×16 cm³ insulated foam boxes covered with reflective foil. Each incubator was sealed with a transparent low-density polyethylene film, which also served as a windscreen. A temperature sensor was mounted directly on the backside of the sample to measure its real-time temperature, recorded continuously by a high-precision multi-channel device with an uncertainty of ±0.01 °C (TOPRIE TP700). For comparison, a similar sensor was placed in the same position to monitor ambient temperature without the sample present. Solar radiation intensity was obtained from the Hong Kong Observatory and measured with an irradiometer (TES1333R, TES Electrical & Electronics, Taiwan, China), which has an accuracy of ±5%, recording the solar radiation outside the box. The experiment took place on a clear day on the flat roof of a five-story building at the Hong Kong University of Science and Technology in Hong Kong.

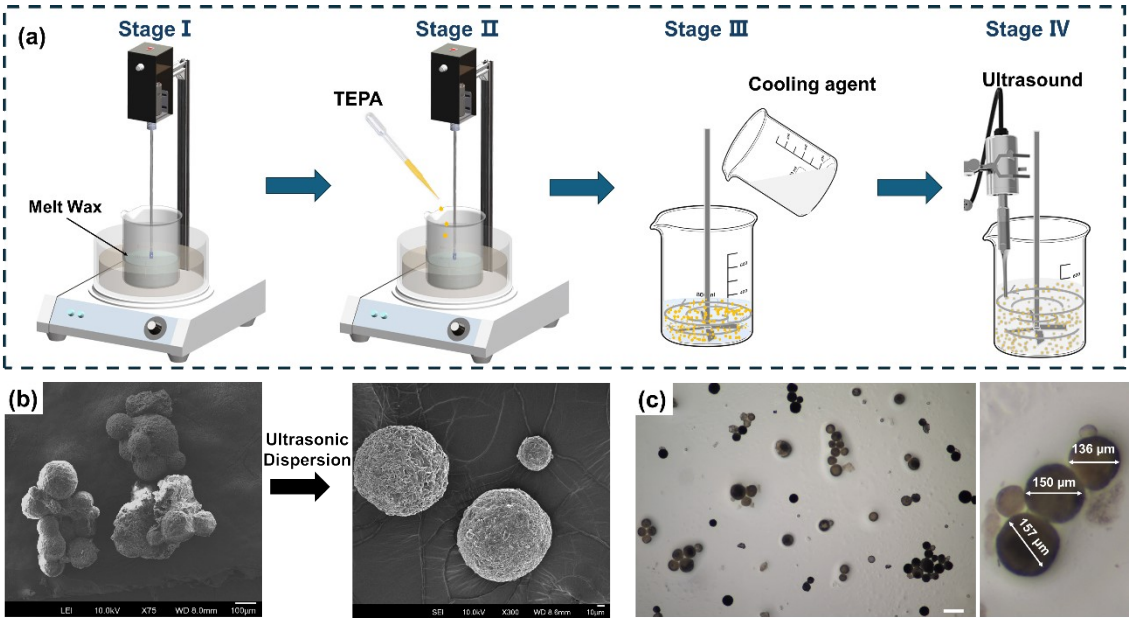

Figure S1 Temperature-controlled phase separation and shell formation induced by the melt condensation method. (a) Schematic of the encapsulation process; (b) The microcapsules, displaying slight adhesion, were dispersed through ultrasonic treatment to obtain distinct individual microcapsules; (c) the microcapsules observed by optical microscopy show a clear sphere, and the diameter is around 150 μm, scale bar =200 μm.

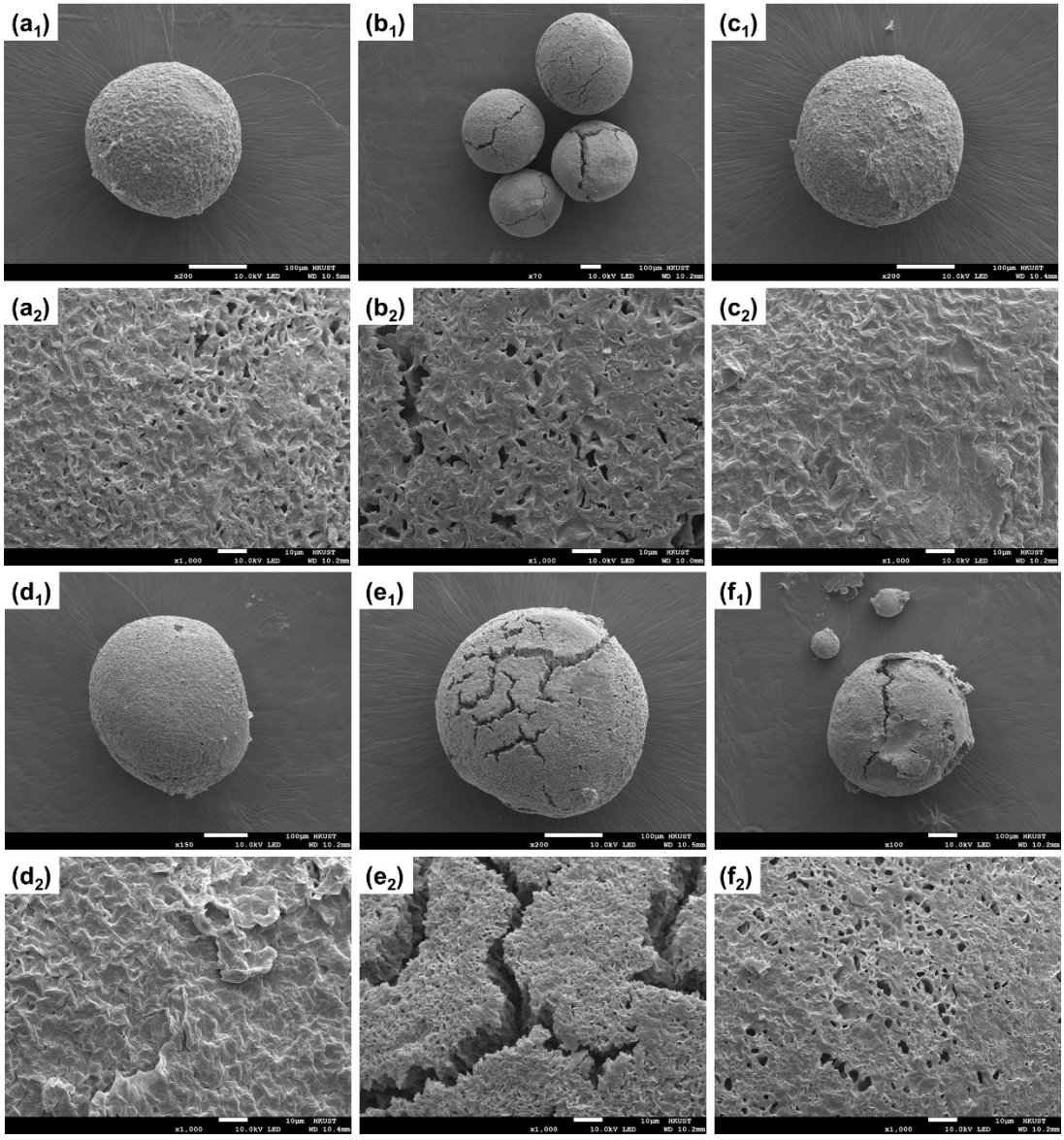

Figure S2 Overall shape and detailed surface morphology of (a) pristine microcapsules without solvents and microcapsules soaking in (b) water; (c) cyclohexane; (c) n-hexane; (e) acetone, and (f) toluene for 48h.

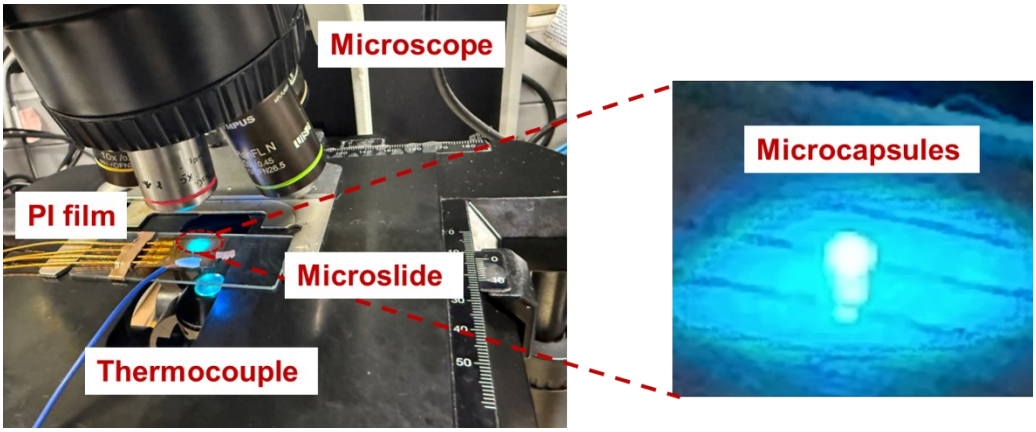

Figure S3 Lab-made heating device to investigate the heat release of microcapsules.

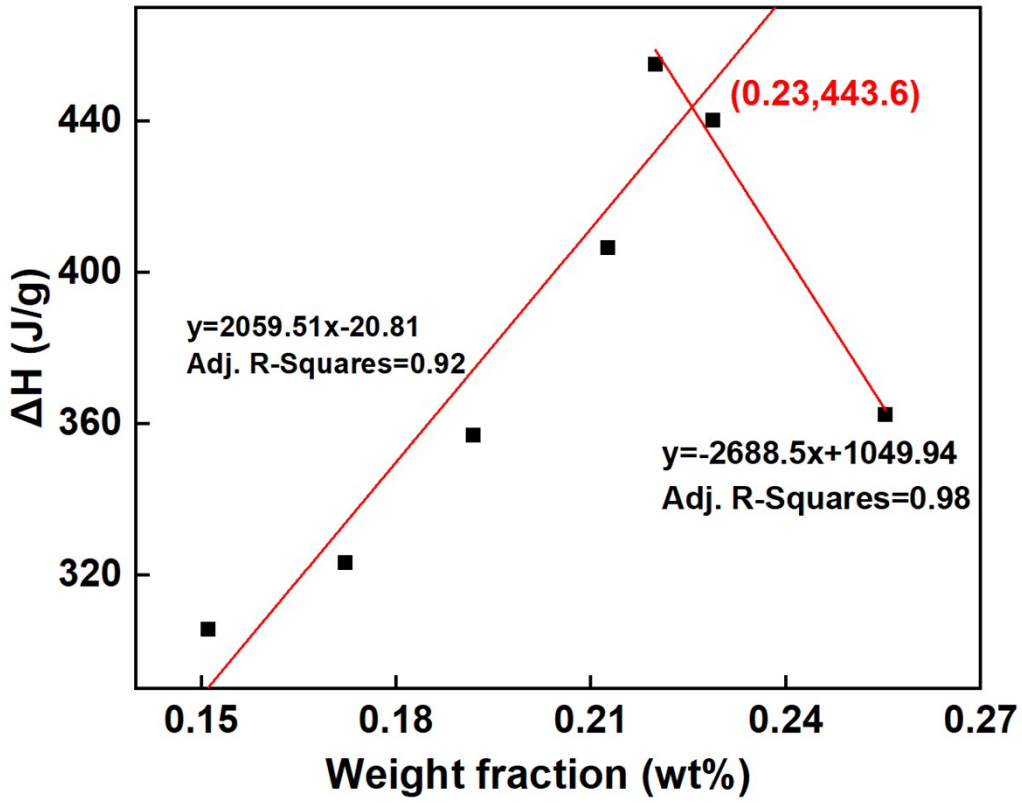

Figure S4 Dependence of reaction heat on different weight fractions of microcapsules in the adhesive.

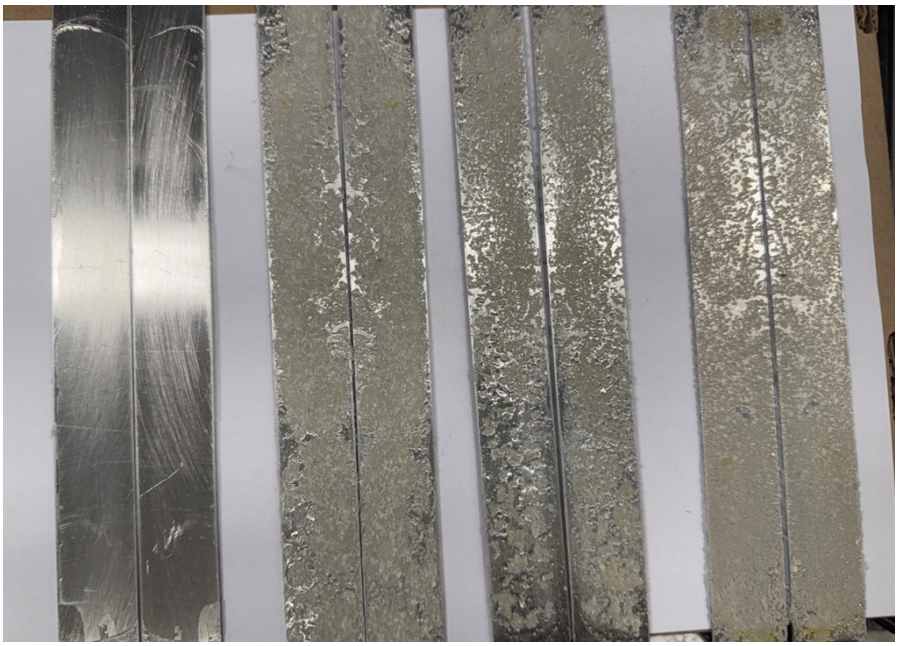

Figure S5 The failure mode transforms in T-peeling tests.

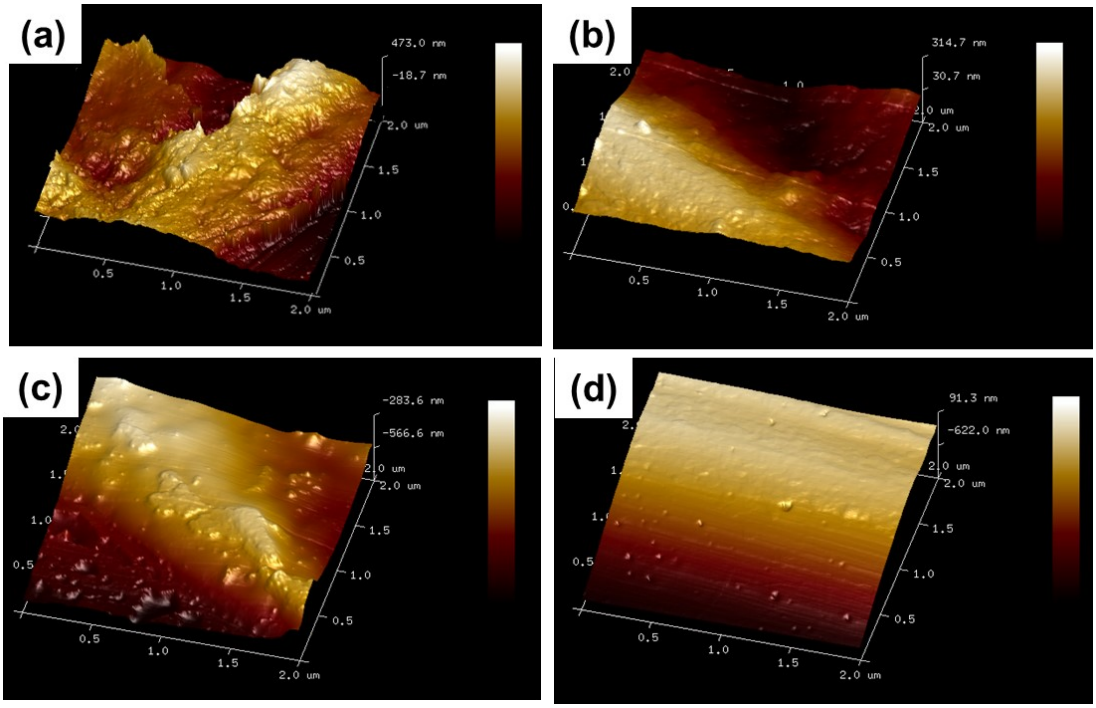

Figure S6 The roughness of the adhesive peel surface between the substrates and the adhesives: (a) Pure A, (b) A-1, (c) A-2, and (d) A-3.

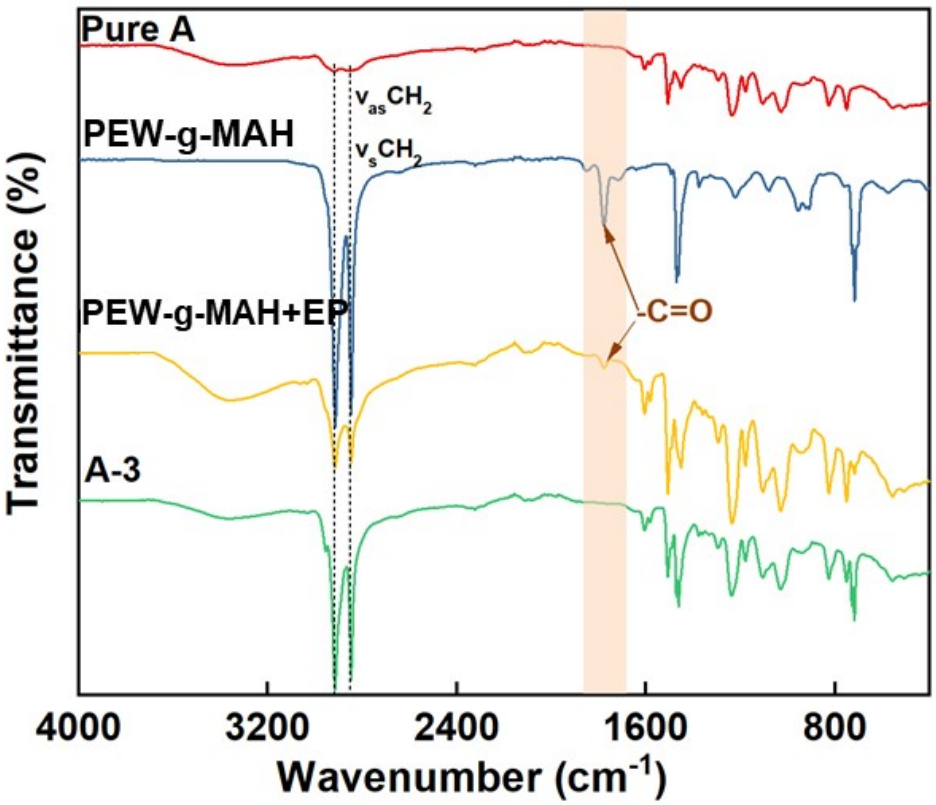

Figure S7 The absence of C=O bonds in A-3 indicated that PEW-g-MAH had participated in the formation of the interpenetrating network.

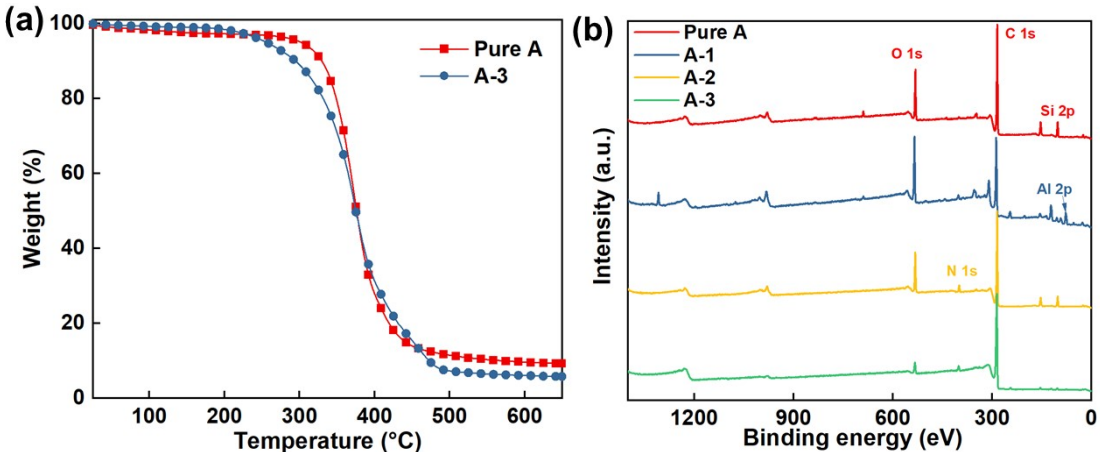

Figure S8 (a) The thermal stability of pure A and A-3; (b) Element analysis of the adhesion surface of aluminum substrates after peeling off the adhesives.

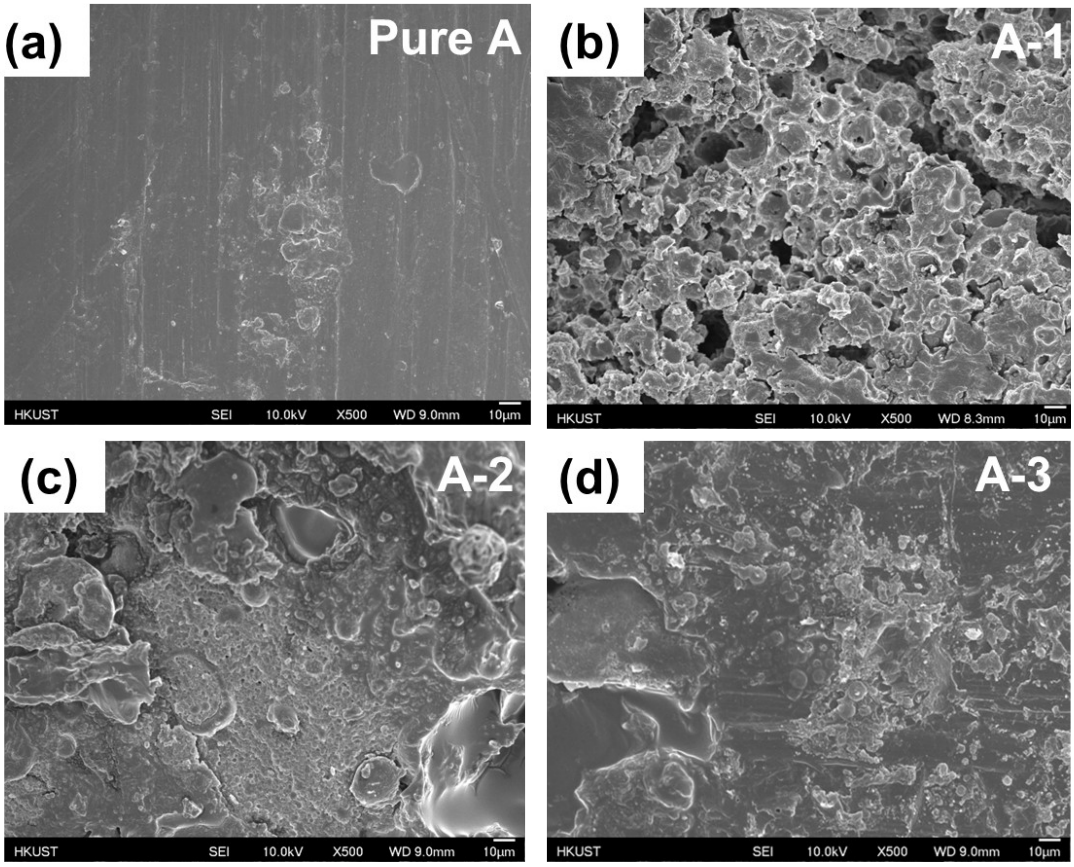

Figure S9 The failure face structure of the adhesives: (a) Pure A, (b) A-1, (c) A-2, and (d) A-3.

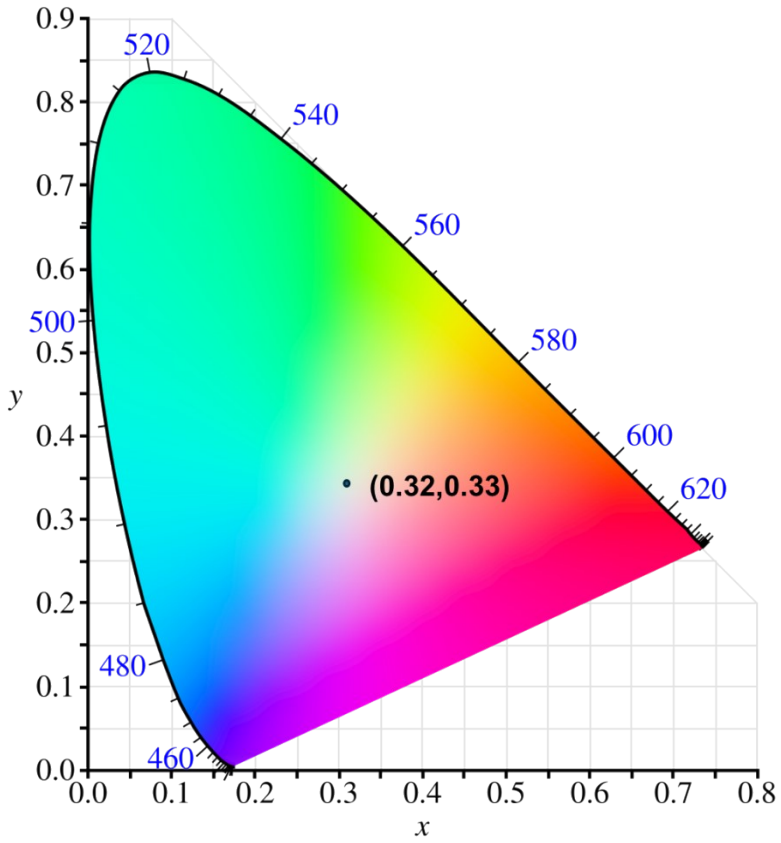

Figure S10 Commission Internationale d'Eclairage (CIE) chromaticity coordinates of the M/EP.

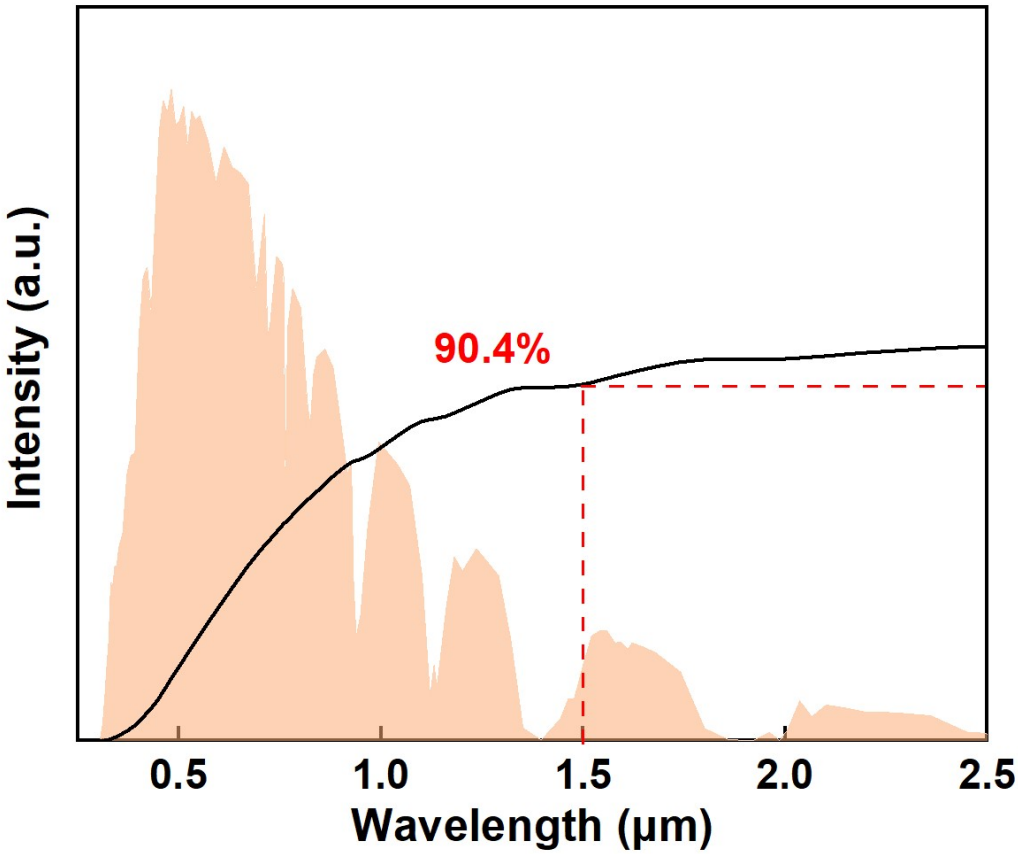

Figure S11 Integral curve of the solar spectrum.

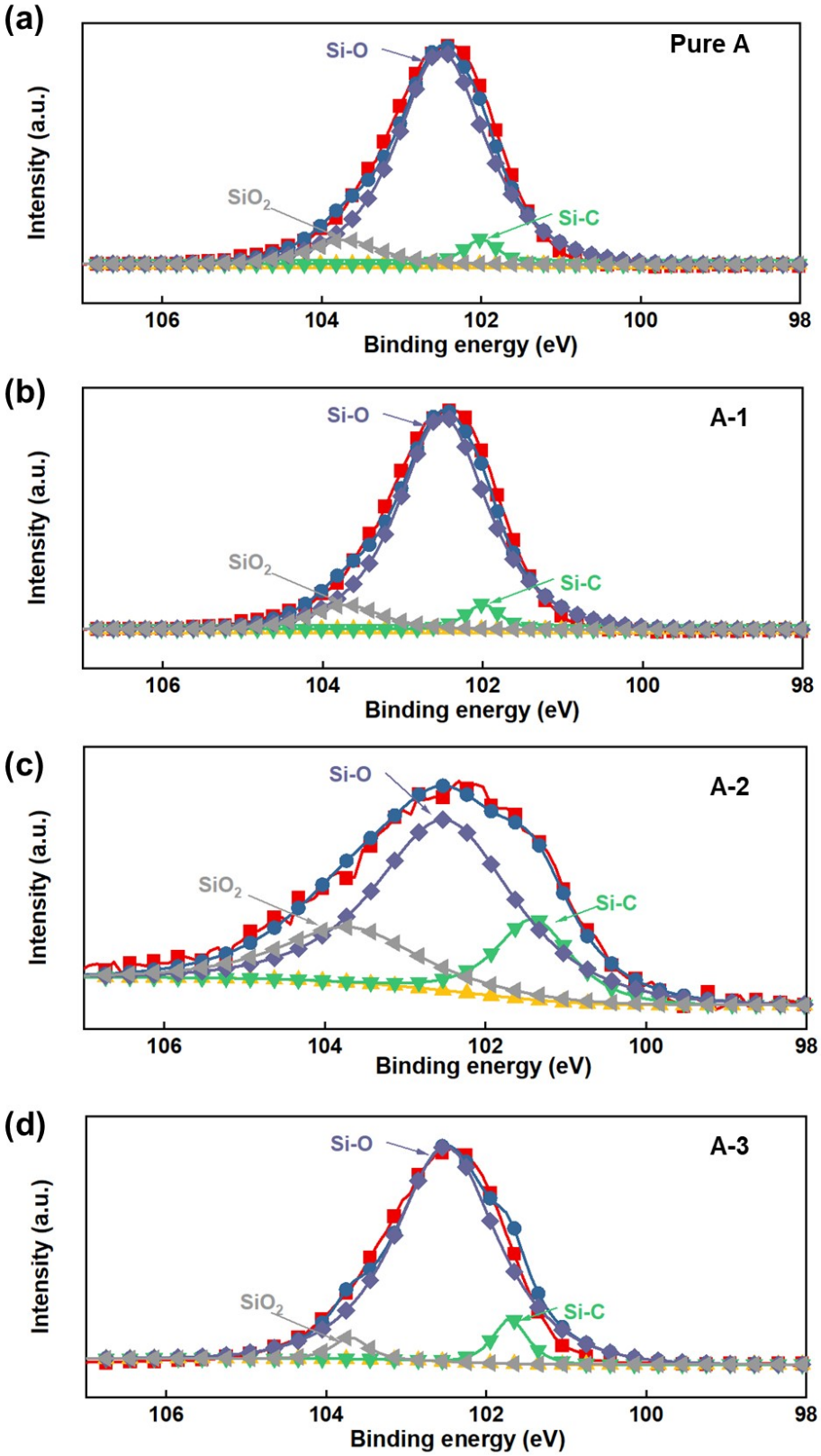

Figure S12 The Si-O, Si-C, and SiO_2 in Epolam 5015 assisted the high radiation rate of one-component coating within the mid-infrared region.

Temperature (°C) \ Relative Humidity %	5	10	15	20	25	30	35	40	45	50	55	60	65	70	75	80	85	90	95	100
46	-2.62	7.11	13.18	17.67	21.26	24.27	26.87	29.16	31.22	33.08	34.79	36.36	37.83	39.2	40.49	41.71	42.86	43.96	45	46
45	-3.32	6.36	12.4	16.86	20.43	23.42	26	28.27	30.31	32.17	33.86	35.43	36.89	38.25	39.53	40.74	41.88	42.97	44.01	45
44	-4.01	5.61	11.61	16.04	19.59	22.56	25.13	27.39	29.41	31.25	32.94	34.5	35.94	37.3	38.57	39.77	40.91	41.99	43.02	44
43	-4.7	4.86	10.82	15.23	18.75	21.7	24.25	26.5	28.51	30.34	32.01	33.56	35	36.34	37.61	38.8	39.93	41	42.02	43
42	-5.4	4.11	10.03	14.41	17.91	20.85	23.38	25.61	27.61	29.43	31.09	32.62	34.05	35.39	36.64	37.83	38.95	40.01	41.03	42
41	-6.09	3.36	9.25	13.6	17.08	19.99	22.5	24.72	26.71	28.51	30.16	31.69	33.11	34.43	35.68	36.86	37.97	39.03	40.04	41
40	-6.79	2.61	8.46	12.78	16.24	19.13	21.63	23.83	25.81	27.6	29.24	30.75	32.16	33.48	34.72	35.89	36.99	38.04	39.04	40
39	-7.49	1.85	7.67	11.96	15.4	18.27	20.76	22.94	24.91	26.68	28.31	29.82	31.22	32.53	33.75	34.91	36.01	37.06	38.05	39
38	-8.19	1.1	6.88	11.15	14.56	17.42	19.88	22.05	24	25.77	27.39	28.88	30.27	31.57	32.79	33.94	35.03	36.07	37.06	38
37	-8.88	0.34	6.09	10.33	13.72	16.56	19.01	21.17	23.1	24.85	26.46	27.95	29.33	30.62	31.83	32.97	34.05	35.08	36.06	37
36	-9.58	-0.41	5.29	9.51	12.88	15.7	18.13	20.27	22.2	23.94	25.54	27.01	28.38	29.66	30.86	32	33.08	34.1	35.07	36
35	-10.28	-1.17	4.5	8.69	12.04	14.84	17.25	19.38	21.29	23.02	24.61	26.07	27.43	28.71	29.9	31.03	32.1	33.11	34.08	35
34	-10.99	-1.93	3.71	7.87	11.19	13.98	16.38	18.49	20.39	22.11	23.68	25.14	26.49	27.75	28.94	30.06	31.12	32.12	33.08	34
33	-11.69	-2.68	2.91	7.05	10.35	13.12	15.5	17.6	19.48	21.19	22.75	24.2	25.54	26.79	27.97	29.08	30.14	31.14	32.09	33
32	-12.39	-3.44	2.12	6.23	9.51	12.25	14.62	16.71	18.58	20.27	21.83	23.26	24.59	25.84	27.01	28.11	29.16	30.15	31.1	32
31	-13.09	-4.2	1.33	5.41	8.66	11.39	13.74	15.82	17.67	19.36	20.9	22.32	23.65	24.88	26.05	27.14	28.18	29.16	30.1	31
30	-13.8	-4.96	0.53	4.58	7.82	10.53	12.87	14.93	16.77	18.44	19.97	21.39	22.7	23.93	25.08	26.17	27.2	28.18	29.11	30
29	-14.5	-5.72	-0.27	3.76	6.98	9.67	11.99	14.03	15.86	17.52	19.04	20.45	21.75	22.97	24.12	25.2	26.22	27.19	28.12	29
28	-15.21	-6.48	-1.06	2.94	6.13	8.8	11.11	13.14	14.96	16.61	18.12	19.51	20.8	22.01	23.15	24.22	25.24	26.2	27.12	28
27	-15.92	-7.25	-1.86	2.11	5.29	7.94	10.23	12.25	14.05	15.69	17.19	18.57	19.86	21.06	22.19	23.25	24.26	25.22	26.13	27
26	-16.63	-8.01	-2.66	1.29	4.44	7.08	9.35	11.35	13.14	14.77	16.26	17.63	18.91	20.1	21.22	22.28	23.28	24.23	25.14	26
25	-17.33	-8.77	-3.46	0.46	3.59	6.21	8.47	10.46	12.24	13.85	15.33	16.69	17.96	19.15	20.26	21.31	22.3	23.24	24.14	25
24	-18.04	-9.54	-4.26	-0.36	2.75	5.35	7.59	9.56	11.33	12.93	14.4	15.75	17.01	18.19	19.29	20.33	21.32	22.26	23.15	24
23	-18.75	-10.3	-5.06	-1.19	1.9	4.48	6.71	8.67	10.42	12.01	13.47	14.81	16.06	17.23	18.33	19.36	20.34	21.27	22.15	23
22	-19.47	-11.07	-5.86	-2.02	1.05	3.62	5.83	7.77	9.52	11.09	12.54	13.88	15.12	16.27	17.36	18.39	19.36	20.28	21.16	22
21	-20.18	-11.83	-6.66	-2.84	0.2	2.75	4.94	6.88	8.61	10.18	11.61	12.94	14.17	15.32	16.4	17.42	18.38	19.3	20.17	21
20	-20.89	-12.6	-7.46	-3.67	-0.65	1.88	4.06	5.98	7.7	9.26	10.68	12	13.22	14.36	15.43	16.44	17.4	18.31	19.17	20
19	-21.6	-13.37	-8.26	-4.5	-1.5	1.01	3.18	5.08	6.79	8.34	9.75	11.06	12.27	13.4	14.47	15.47	16.42	17.32	18.18	19
18	-22.32	-14.14	-9.07	-5.33	-2.35	0.15	2.3	4.19	5.88	7.41	8.82	10.11	11.32	12.44	13.5	14.5	15.44	16.33	17.19	18
17	-23.03	-14.91	-9.87	-6.16	-3.2	-0.72	1.41	3.29	4.97	6.49	7.89	9.17	10.37	11.49	12.53	13.52	14.46	15.35	16.19	17
16	-23.75	-15.68	-10.67	-6.99	-4.05	-1.59	0.53	2.39	4.06	5.57	6.96	8.23	9.42	10.53	11.57	12.55	13.48	14.36	15.2	16
15	-24.47	-16.45	-11.48	-7.82	-4.9	-2.46	-0.36	1.49	3.15	4.65	6.03	7.29	8.47	9.57	10.6	11.58	12.5	13.37	14.2	15
14	-25.19	-17.22	-12.28	-8.65	-5.75	-3.33	-1.24	0.6	2.24	3.73	5.09	6.35	7.52	8.61	9.64	10.6	11.52	12.38	13.21	14
13	-25.9	-17.99	-13.09	-9.48	-6.6	-4.2	-2.13	-0.3	1.33	2.81	4.16	5.41	6.57	7.65	8.67	9.63	10.54	11.4	12.22	13
12	-26.62	-18.77	-13.9	-10.31	-7.46	-5.07	-3.01	-1.2	0.42	1.89	3.23	4.47	5.62	6.69	7.7	8.65	9.55	10.41	11.22	12
11	-27.35	-19.54	-14.71	-11.15	-8.31	-5.94	-3.9	-2.1	-0.49	0.96	2.3	3.53	4.67	5.73	6.74	7.68	8.57	9.42	10.23	11
10	-28.07	-20.31	-15.51	-11.98	-9.16	-6.81	-4.78	-3	-1.4	0.04	1.36	2.58	3.72	4.78	5.77	6.71	7.59	8.43	9.24	10
5	-31.69	-24.2	-19.56	-16.16	-13.44	-11.17	-9.22	-7.5	-5.97	-4.58	-3.3	-2.13	-1.04	-0.02	0.93	1.83	2.69	3.5	4.27	5
0	-35.33	-28.1	-23.63	-20.35	-17.73	-15.55	-13.67	-12.02	-10.54	-9.2	-7.98	-6.85	-5.8	-4.82	-3.91	-3.04	-2.22	-1.45	-0.71	0

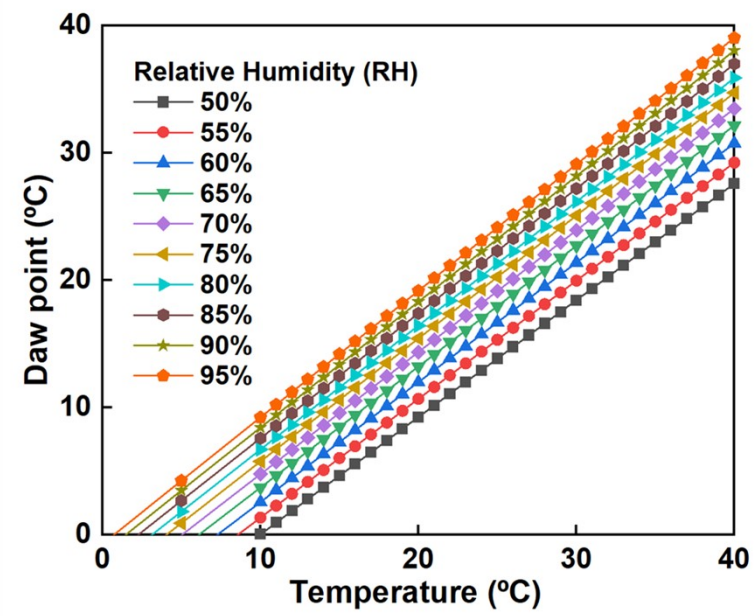

Figure S13 Relationship between temperature, dew point, and relative humidity. The yellow area indicates the climate conditions where condensation may occur on the surface of M/EP when it is exposed to actual weather (https://www.mrfixitbali.com/images/articleimages/dew-point-chart-full.pdf).

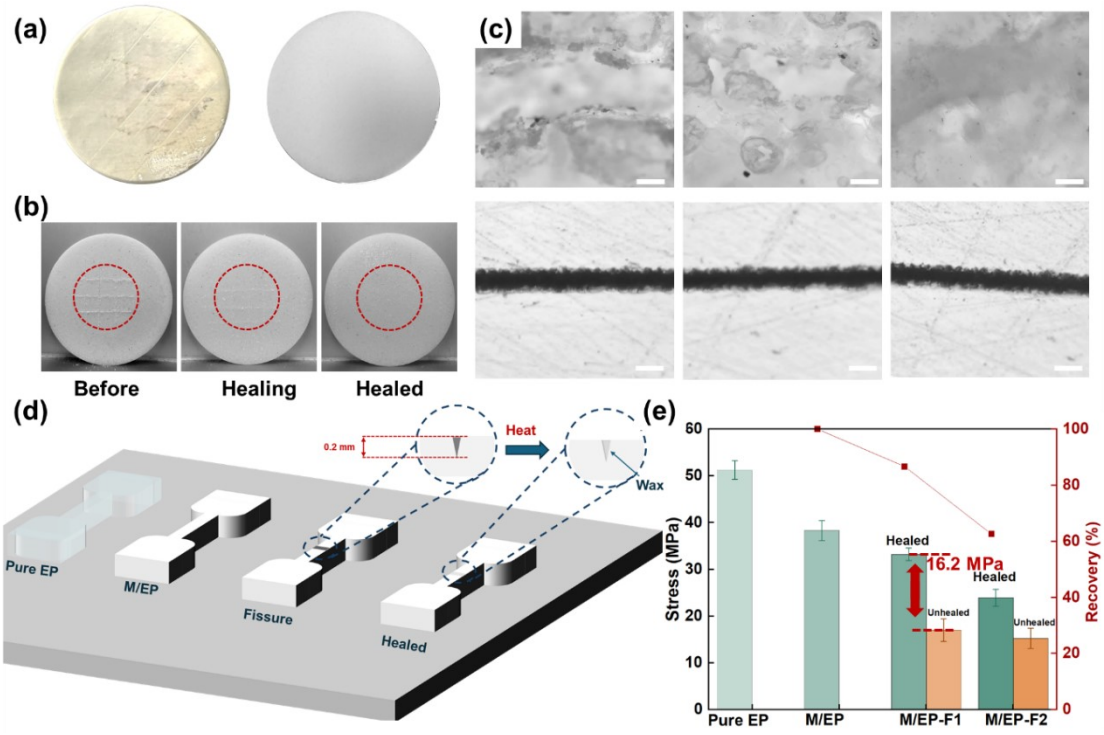

Figure S14 Self-healing performance of prepreg formulated with an epoxy matrix and TEPA microcapsules. (a) Comparison between transparent pure epoxy polymer and white microcapsule-infused epoxy polymer; (b) scratch-healing process of the M/EP composite coating; (c) microscopic examination of the M/EP composite coating (upper) and the pure EP composite coating (bottom) during the scratch-healing process; (d) diagram illustrating the recovery test for the M/EP composite coating; (e) tensile strength and recovery performance of pure EP, as well as M/EP composites, with and without healing capabilities.

Table S1: The double emulsion system used for adjusting the interface tension

Group	Phase A	Phase B	Phase C
1	TEPA	85 wt% PEW+15 wt% PEW-g-MAH	PFTBA
2		90 wt% PEW+10 wt% PEW-g-MAH	
3		95 wt% PEW+5 wt% PEW-g-MAH	
4		PEW+3 wt% Span 80	
5		PEW+3 wt% Arlacel P135	
6		PEW+3 wt% Span 85	

Table S2 Data related to energy-saving calculations.

ID	FQ	sample	check group	Saving (GJ)	Cooling power saving (MJ/m2)	Energy saving ratio (%)
1	Af	321.7	357.6	35.9	14.4	10.0
2	Am	151.9	173.5	21.6	8.7	12.5
3	Aw	281.8	314.8	33.0	13.2	10.5
4	Bsh	111.2	134.0	22.8	9.1	17.0
5	Bsk	43.9	55.9	12.0	4.8	21.5
6	Bwh	99.7	117.3	17.5	7.0	15.0
7	Bwk	104.9	121.4	16.5	6.6	13.6
8	Cfa	65.2	74.4	9.2	3.7	12.4
9	Cfb	2.3	3.7	1.4	0.6	37.8
10	Cfc	0	0	0	0	0
11	Csa	18.7	26.3	7.5	3.0	28.8
12	Csb	2.2	4.5	2.3	0.9	50.4
13	Csc	0	0	0	0	0
14	Cwa	159.1	177.6	18.5	7.4	10.4
15	Cwb	0.04	0.3	0.3	0.1	85.7
16	Cwc	0	0	0	0	0
17	Dfa	19.2	24.7	5.5	2.2	22.2
18	Dfb	0.9	2.1	1.1	0.5	55.1
19	Dfc	0	0.09	0.09	0.04	100
20	Dfd	1.2	3.2	2	0.8	62.3
21	Dsa	21.1	26.8	5.7	2.3	21.2
22	Dsb	362.8	406.3	43.5	17.4	10.7
23	Dsc	0	0	0	0	0
24	Dsd	0	0.2	0.2	0.08	100
25	Dwa	42.2	51.6	9.4	3.8	18.2

26	Dwb	0.02	0.3	0.3	0.1	93.3
27	Dwc	0.1	0.6	0.5	0.2	77.2
28	Dwd	0	0	0	0	0
29	EF	0	0	0	0	0
30	ET	0	0	0	0	0

Table S3 Healing effect of the M/EP samples.

Sample	**Strength (MPa)**	**Modulus (GPa)**	**Healing Efficiency***
Pure epoxy	51.2 ± 2.0	2.9 ± 0.1	N/A
M/EP	38.3 ± 2.1	2.6 ± 0.2	N/A
M/EP-1 healed	33.2 ± 1.3	2.3 ± 0.1	86.7%
M/EP-1 without healing	17.0 ± 2.4	2.1 ± 0.2	N/A
M/EP-2 healed	23.9 ± 1.8	2.3 ± 0.1	62.6 %
M/EP-2 without healing	15.2 ± 2.2	2.1 ± 0.2	N/A

*Healing efficiency = (healed strength / Original composite strength) × 100%